

# Mechanistic aspects of selective laser patterning of multilayered thin-film structures in OLED fabrication

*Dimitris Karnakis*

*Oxford Lasers Ltd, Unit 8 Moorbrook Park, Didcot Oxfordshire OX11 7HP United Kingdom*

*Geert Van Steenberge, An Gielen, Johan De Baets*

*Ghent University-IMEC, Department of Electronics and Information Systems, Centre for Microsystems Technology, Technologiepark 914A, B-9052 Ghent, Belgium*

*Jeroen van den Brand*

*Holst Centre, High Tech Campus 31, 5656 AE Eindhoven, The Netherlands*

## **Abstract**

*Selective laser patterning of OLEDs on flexible substrates represents a novel optical engineering challenge. Here we discuss the potential of ultrafast diode-pumped solid-state (DPSS) and UV excimer lasers for this application and demonstrate a stable process window for large area OLED patterning. We specifically studied the removal of transparent conductive layers on barrier layer and metal electrodes on active OLED layer and report on laser damage thresholds, resulting feature quality and process speed limitations. Careful examination with optical profilometry and SEM reveals that the choice of laser wavelength and more importantly laser pulse duration is key for this application. A photomechanical stress-induced ablation mechanism is believed to be driving this process, resulting in debris-free, low temperature patterning with demonstrably no detrimental effects to the OLED performance.*

## **1. Introduction**

Organic LEDs have attracted a tremendous interest due to their potential in display applications or as energy-efficient solid-state light sources [1-3]. For lighting and signage applications in particular, white OLEDs can potentially revolutionise this industry. Polymer LEDs are compatible with fabrication processes in ambient conditions and hence are ideally suited to low-cost roll-to-roll (R2R) manufacturing. Such production technology is currently favoured for making OLEDs for lighting on large-area flexible substrates [4] but is not entirely problem-free. Among the first technological barriers to be overcome is the development of a barrier technology capable of preventing ingress of water and oxygen, which damages OLEDs [5]. But equally important is the choice of suitable layer deposition and post-patterning techniques to ensure uniform, cost-effective and stable production which is also fully protective of the barrier layer. Several patterning techniques (wet chemical, soft lithography, laser) have been evaluated, each with its own drawbacks [6-10]. This paper describes in some detail the use of laser technology for OLED fabrication on foil, which presents a novel optical engineering challenge and discusses the mechanistic aspects in laser thin-film ablation. The complexity of this task arises mainly from the requirement for ultra-precise selective layer patterning of several different layer combinations in an OLED stack, each with widely varying optical and thermal properties. Although lasers should not be considered as a panacea to this problem,

they do offer distinct advantages comparing to other patterning technology. Especially as, they represent a non-contact, fast, dry process which is easily scalable and easily integrated with R2R technology.

The key requirements for large-area uniform selective layer patterning in OLED fabrication are: (a) removing completely single or multiple stack layers without any remaining residue, (b) capturing all removed material above the patterned surface while avoiding any contamination from redeposited debris and (c) maintaining the integrity and functionality of all layers in the stack without loss in performance.

With an appropriate choice of laser, all three criteria can be fulfilled. It is essential that laser structuring must proceed via a low temperature removal mechanism, suppressing any thermal characteristics that could potentially damage the heat sensitive OLED or barrier layers, while also containing laser debris. This can be preferably accomplished using short-pulsed lasers via a stress-assisted (film fracture and ejection) ablation mechanism rather than vaporization or other phase change. Our aim here is to quantify the potential of nanosecond UV excimer and picosecond pulse duration DPSS lasers for patterning ITO on the barrier layer and the cathode on polymer LEP and ideally determine a process window for large-area selective OLED patterning.

## **2. Selective laser patterning by stress-assisted ablation**

For stress-assisted laser ablation to occur two important criteria must be fulfilled in any absorbing layer [11]: "thermal confinement" and "stress confinement" (Fig.1). In simple terms, these require that (i) a maximum energy load in the irradiated film is attained from high photon absorption and minimum thermal conduction losses away from the irradiated area and that (ii) rapid laser heating produces a high transient thermoelastic stress that exceeds the film fracture limit before any thermal expansion allows for stress relaxation. The choice of, both, laser wavelength and laser pulse duration are critical as the former controls laser absorption and the latter directly compares with the material's relaxation timescales.

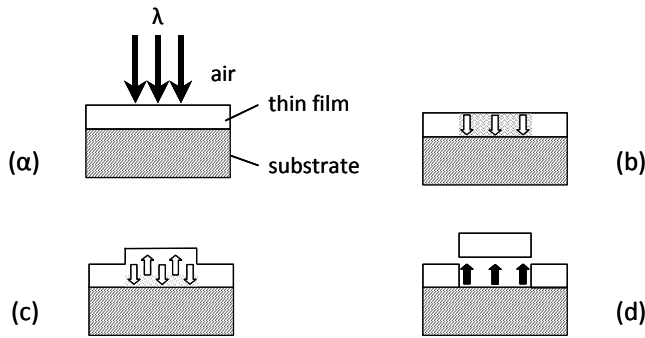


Figure 1 Schematic representation of stress-assisted film ablation on a substrate layer; (a)  $t=0$ , light absorption, (b) rapid laser heating under thermal and stress confinement, maximum compressive thermoelastic stress (c) thermal expansion relaxation with tensile stress generation, (d) tensile strength exceeded, film fracture and ejection

The laser pulse duration must be chosen carefully considering two important material characteristic times: (i) the *thermal relaxation time*  $\tau_{\theta}$  i.e. the time needed to dissipate heat generated by the laser pulse, given by  $\tau_{\theta}=\delta^2/4\chi$  and (ii) the *acoustic relaxation time*  $\tau_A$ , i.e. the time needed to initiate a collective motion of atoms or molecules within the absorbing volume, given by  $\tau_A=\delta/C$ . Here,  $\delta$  refers to the smallest dimension of the heated volume. In our case that is either the film thickness, optical or thermal penetration depth assuming a much larger comparatively irradiating spot size. The remaining parameters are the film thermal diffusivity,  $\chi$  and the sound speed in the film,  $C$ . If the laser pulse duration  $\tau$  is shorter than the thermal relaxation time  $\tau_{\theta}$  ( $\tau<\tau_{\theta}$ ), the thermal confinement criterion is fulfilled maximising the temperature in the heated volume by restricting thermal diffusion to the substrate layers and efficiently generating thermoelastic stress. Additionally, if the laser pulse duration is shorter or comparable to the characteristic acoustic relaxation time  $\tau_A$  ( $\tau<\tau_A$ ), laser heating of the target will proceed at nearly constant volume. The heated material will have little time to expand and the large temperature gradients will cause a buildup of high compressive stresses. The interaction of the laser-induced compressive stresses with the free surface of the irradiated sample can then result in generation of tensile stresses, sufficiently high, that can overcome the dynamic strength of the material causing mechanical fracture or in some cases promote cavitation and fragmentation in a metastable liquid [12]. With this approach differences in thermal expansion between the stack layers can be neglected as the strain is assumed negligible. Note that any stresses existing in the material from the deposition processes are considered negligible in comparison and not accounted for.

### 3. Experimental

A schematic drawing of the complete multilayered OLED stack on foil under investigation is illustrated in figure 2. The sample consisted of a 130nm thick sputtered ITO anode layer on a barrier stack of alternating SiN-organic layers on 100 $\mu$ m thick PEN foil. The 100nm thick Al cathode was thermally evaporated on 80nm thick white LEP (Merck Chemicals) and 100nm thick poly3,4-ethylenedioxythiophene polystyrenesulfonate (PEDOT:PSS, Agfa Orgacon). These organic layers

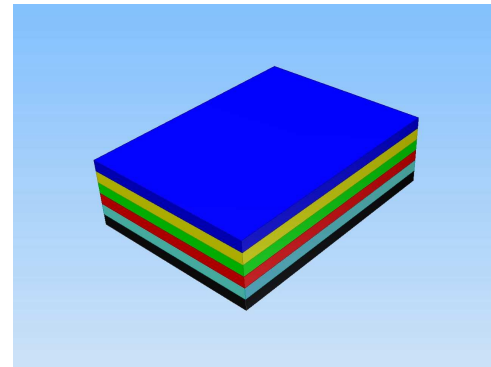


Figure 2 Flexible OLED stack on foil. From bottom upwards the stacklayers are: (black) PEN; (light blue) barrier layer; (red) ITO anode; (green) PEDOT:PSS; (yellow) white LEP and (blue) Ba/Al cathode layer

were sequentially printed on the ITO anode. All laser sources used in this work are commercially available. For ITO patterning on barrier, a direct-write Oxford Lasers Picolase 1000 micromachining system was used (355nm, FWHM 10ps) with a DPSS mode-locked amplifier. The laser repetition rate was fixed at 10kHz. The beam was focused to a spot diameter ( $1/e^2$ ) of 32 $\mu$ m with an f-theta telecentric lens ( $f=100$ mm) and was translated across the ITO surface using a two-axis galvanometer scanner. A UV excimer laser station (248nm, 7ns FWHM) was also used in comparison for ITO patterning equipped with a 0.1NA objective and mask imaging setup. For cathode patterning on white LEP, a Coherent Talisker 532-8 picosecond mode-locked amplifier was used at 532 nm. A direct-write beam delivery setup was used to focus the beam to a 35 $\mu$ m diameter ( $1/e^2$ ) spot. Single or multiple pulse exposure ablation tests were conducted by controlling the incident number of laser pulses per area. Ablation took place in ambient air and a vacuum extraction system removed ablation products above the target. The ablated samples were investigated with SEM, optical microscopy or white-light interferometer.

## 4. Results and Discussion

### 4.1. Laser patterning of ITO on barrier layers

#### 4.1.1. UV excimer laser patterning

Ablation of ITO on barrier was investigated with a 248nm excimer laser in the fluence range 40-180mJ/cm<sup>2</sup> (Fig.3).

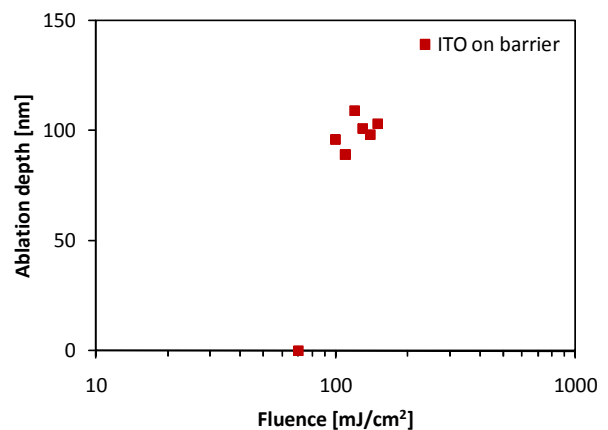


Figure 3 Etch depth versus laser fluence for single-pulse ablation of ITO on barrier (248nm)

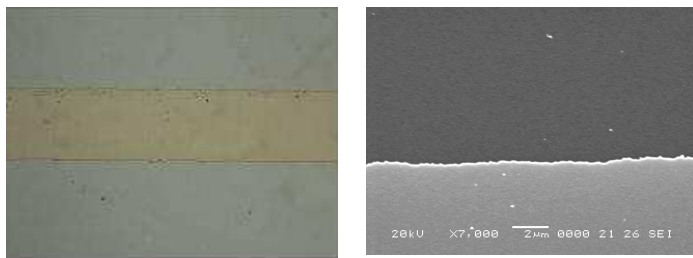


Figure 4 (left) Optical microscope image of a 248nm laser scribed line on ITO/barrier 160mJ/cm<sup>2</sup>, pulse overlap 1.56 pulses per area; (right) Higher magnification SEM image of the ITO scribed line showing a clean ITO edge (light grey) and debris-free barrier underlayer floor (dark grey) Bar denotes 2μm

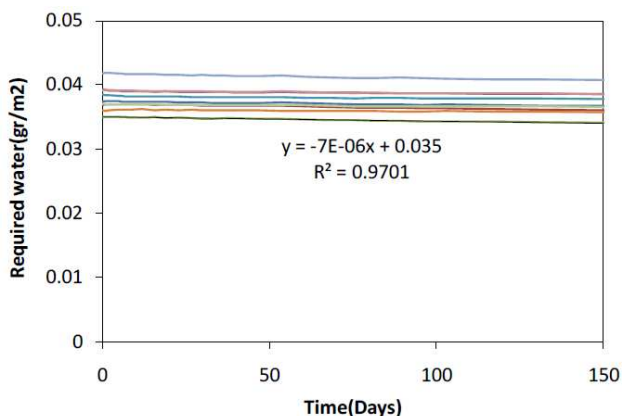


Figure 5 Ca test; Water vapour transmission rate (WVTR) measurement versus time for laser patterned ITO (248nm) on a multilayer barrier stack

The single-pulse ablation threshold was found around 70mJ/cm<sup>2</sup>. But an optimum working fluence for uniform ITO removal on barrier was identified between 120- 160mJ/cm<sup>2</sup> as incomplete ablation was observed across the laser spot size below these values. Optical and SEM images of typical ablation craters are shown in Figure 4. The ITO film has been removed cleanly exhibiting sharp edges with no delamination and no evident damage to the nitride barrier layer. No redeposited debris is detected in the crater vicinity either. This picture changed though with increasing the laser pulse overlap on target. For all investigated fluences, ITO ablation with a higher pulse overlap of 66% or more was accompanied by surface cracking of the underlying SiN layer, most probably due to the increased thermal load in the overlapping regions. No cracking was observed with moderated pulse overlaps of 50% instead.

For an initial characterisation of the barrier layers integrity following ITO laser patterning, the Ca test was used [13]. During this diagnostic test, a well-defined calcium layer was applied on the patterned stack on PEN foil and subsequently covered with a transparent encapsulant. Optical transmission measurements as a function of time, in ambient conditions (20°C, RH50%), provided information on the permeability of the encapsulant and substrate for water and oxygen. Any degradation in the thin-film encapsulant/barrier quality is expected to raise the water vapour transmission rate (WVTR) above the recorded one before laser patterning (<10<sup>-6</sup> g/m<sup>2</sup>/day). Several laser conditions were investigated,

including different laser fluences (120, 140 and 160 mJ/cm<sup>2</sup>), at low pulse overlaps (14.5% and 36%) and compared with non-patterned ITO on a multilayer barrier stack. The results are shown in figure 5, which presents the required water (g/m<sup>2</sup>) as a function over time, corresponding to the measured optical transmission of the calcium layer. The slope of all plotted curves, corresponding to different laser settings, is identical, indicating a WVTR of 10<sup>-6</sup>, which matches well that of the unirradiated multilayer barrier stack. This preliminary result is extremely encouraging indicating that excimer laser patterning does not appear to affect the barrier layer integrity.

#### 4.1.2. Ultrafast DPSS laser patterning

Line patterning of ITO was also examined with the 355nm ultrafast laser for a range of incident laser fluences at different pulse overlaps. Single-pulse ablation of ITO at 355nm starts at 50mJ/cm<sup>2</sup>. Below this value, no ablation was recorded. At higher fluences between 75-130mJ/cm<sup>2</sup>, ITO ablation resulted also in surface roughening of the underlying SiN barrier layer.

Figure 6 shows an optical image of an interrupted laser scribed line in ITO using low pulse overlap and low fluence (62mJ/cm<sup>2</sup>) to illustrate the ablation character of this process. Discrete irregularly-shaped ablated craters are observed aligned in the direction of scanning. It is interesting that the ablated films appear to have been removed intact with no damage to the underlying SiN layer. There is also no evidence for melting or any other phase-change and by and large, no debris was found scattered in or around the craters, suggesting that ITO and the barrier layers have probably experienced a very low temperature rise from the laser interaction. The fractured morphology of these craters reveals the photo-mechanical character of ablation here. This is particularly evident near certain crater edges, where incomplete ablation has resulted in lifted-off ITO flakes. These remain still attached to the parent film but are clearly not thermally decomposed. Very few (badly extracted) ablated layers, were found redeposited nearby the craters (not shown here) as softened curled up flakes, supporting this view further.

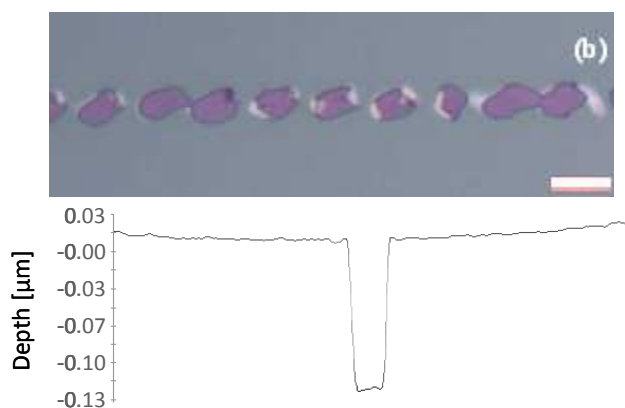


Figure 6 Optical image of 355nm 10ps laser (non-continuous) scribed line in ITO (grey) on barrier (purple) at 62 mJ/cm<sup>2</sup>. White bar denotes 9μm. Optical profiler depth measurement of 355nm, 10ps ablated ITO crater; scribed depth: 123nm, crater width: 9-12μm, (Y) scale: 15nm/div

By adjusting the scribing speed, the ablated craters can be joined to form an uninterrupted continuous scribed line on ITO. Depth profile measurements of this line confirm clean ablation with smooth uniform floors, no edge delamination in the adjacent unexposed areas and an etched depth of 123nm indicating that only ITO has been removed leaving the remaining stack unharmed. Furthermore, electrical continuity measurements confirmed that such lines could be used to create electrically isolated OLED tiles.

#### 4.2. Laser patterning of cathode on white LEP

Laser patterning of metal films on polymer substrates is challenging, as typically metal ablation requires higher energy input comparing to ablation of organics. This increases the potential for damage to typically heat or light sensitive organic underlayers. Here, single-pulse ablation of the Ba/Al cathode bilayer on the OLED stack was investigated using a visible (532nm) picosecond pulse duration laser. The wavelength was especially chosen to facilitate a self-limiting ablation process by minimising optical damage from residual absorbed light to any of the underlying stack layers considered almost transparent at 532nm. By contrast the cathode layer absorbs very well at this wavelength ( $\alpha=1.2\times 10^6\text{cm}^{-1}$ ) although the average reflectivity is also quite high at 92%. Additionally, the use of ultrashort (ps) laser pulses is intended to limit any thermally related damage during ablation.

The single-pulse ablation threshold for cathode removal on LEP was measured as  $95\pm 9\text{mJ}/\text{cm}^2$  [14]. This was derived from analysing a series of single-pulse ablated craters with increasing laser pulse energy. Remarkably, laser irradiation with fluences ranging between  $140\text{--}360\text{mJ}/\text{cm}^2$  removed the cathode layer *only*, leaving the LEP surface intact. This represents a narrow but comfortable process window for cathode removal, with a typical example of an ablated crater shown in figure 7. In that case, the incident average (not peak) fluence used was  $230\text{mJ}/\text{cm}^2$ . A uniform reasonably flat floor was recorded by optical profile examination across the  $20\mu\text{m}$  crater diameter. The resulting crater rim shows irregularly shaped edges though, which are folded back towards the adjacent unirradiated surface, contributing to a rim elevation of  $500\text{nm}$ . These irregularly shaped boundaries imply a film rupturing process. It is expected that with a more spatially uniform incident laser beam profile, this effect can be moderated. More interestingly though, there is hardly any (newly introduced) laser-induced surface contamination around the crater such as microdroplets or other debris. That is encouraging and indicative of a low temperature removal process which is also supported by the film rupturing observations.

At higher fluences ( $F>360\text{mJ}/\text{cm}^2$ ), two or more stack layers were ablated simultaneously and the craters were deeper at the centre as expected from a non-uniform profile laser beam. Similarly, multiple pulse irradiation even at low fluence created deeper craters by removing the underlying LEP and Pedot:PSS organic layers as well. In both cases, the stepped ablation craters indicate a deterministic character in the removal process. The craters remained quite sharp with clean edges even at the highest examined fluence of  $825\text{mJ}/\text{cm}^2$ .

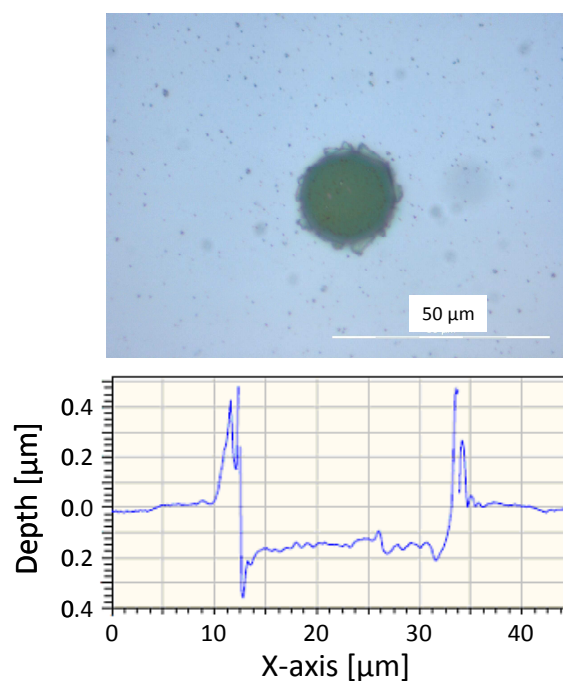


Figure 7 (top) Optical microscope image of single-pulse ps laser ablated cathode crater on LEP 532nm, 10ps, 2.5 $\mu\text{J}$ ; Bar 50 $\mu\text{m}$ , (bottom) Depth profile of the ablated crater, recorded depth~140nm. Scale (X): 2.5 $\mu\text{m}/\text{div}$ , (Y):25nm/div

Unlike nanosecond UV ablation of metals [15] where the ablated films are usually “blown off” in liquid phase via a substrate assisted explosive removal, picosecond laser patterning here was shown to permit precise metal removal with little, if any, melting involved and generally limited thermal damage characteristics. An exact mechanism for the clean metal removal is still not entirely clear.

With an optical penetration depth of only 8.3nm, any laser heating of the film should be dictated by thermal diffusion during the laser pulse. Since the thermal response of metals to ultrafast excitation is a two-step non-equilibrium process, different electron and lattice heating rates apply and the classical square root dependence of heat diffusion on laser pulse duration is not valid anymore. It is expected that the incident laser energy is initially absorbed by electrons during excitation and, soon after, a portion of that is transferred to the lattice through electron-phonon coupling. Meanwhile, hot electrons diffuse deeper in the material extending the heated depth. Our approximation of the electron penetration distance before lattice coupling in the cathode, based on [16], is  $\approx 72\text{nm}$  using an electron-phonon coupling constant for Al of  $3.1\times 10^{17}\text{W}/\text{m}^3\text{K}$  [17] and a weaker dependence on laser pulse duration  $\tau^{0.2}$ .

With  $\delta=72\text{nm}$ , the estimated thermal and acoustic relaxation times are almost equal at  $\tau_{\theta}\approx\tau_A=13\text{ps}$  and marginally higher than the 10ps laser pulse duration. Since therefore, both thermal and stress confinement criteria are satisfied, the metal layer will become highly compressed upon laser heating. At low fluences, a hot-electron blast force is expected to generate a shock wave early on, that weakens the material. This is compounded by the thermal load from the

subsequent lattice heating after the laser pulse which could generate enough thermoelastic stress to exceed upon relaxation an expected tensile strength for Al of 450MPa [18] and result in film fracture even below the Al melting point of 933K. Such a qualitative explanation can support the macroscopically observed lack of both cathode melting and thermal damage on the underlying LEP layer during low power picosecond laser patterning.

It should also be mentioned that the cathode layer adhesion on LEP is expected to be rather poor. This should help to remove the layer relatively easily, although the estimated energy density requirements to exceed the adhesion strength is negligible compared to the observed ablation threshold. The cathode layer ejection mechanism might also be substrate-assisted. As the back surface of the cathode becomes progressively hotter, diffusing heat could moderately raise the temperature of the LEP layer in contact. It is plausible, assuming a slow “heat leaking” rate from LEP to the PEDOT:PSS layer underneath, that such a temperature rise could cause local thermal expansion of the LEP and generate enough pressure behind the metal film that could contribute (together with internal stress) to the detachment of the softer cathode layer. Observed permanent damage from LEP surface swelling at slightly higher fluences could support such contribution to the cathode ablation route. Further experimental evidence exploring the timescale of ablation on such multilayered OLED stacks could help clarify the cathode ejection mechanism further.

## 5. OLEDs for lighting

Initial efforts to demonstrate compatibility to laser structuring have resulted in the fabrication of a prototype white OLED device on glass (figure 8). ITO and Al/Ba were used as the anode and cathode respectively. The photograph shows an OLED plate of which only one of the individual devices has been switched on. All other devices on the plate worked also. Although not visible in the picture, the devices showed some small blackspots which is due to exposure of the OLED device to the ambient during processing. Future developments therefore include laser processing in protective environments to prevent such damage.

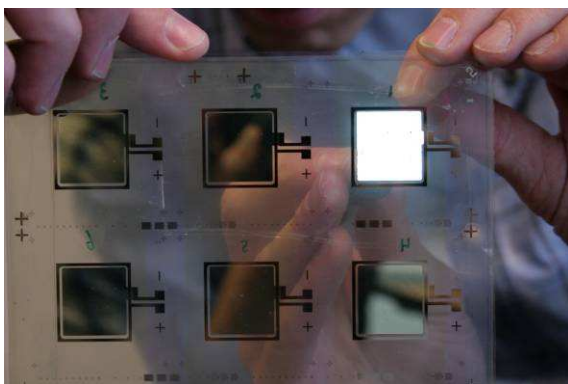


Figure 8 Test OLED device on glass incorporating laser structuring of ITO anode and Al cathode.

## 6. Summary

Experimental evidence suggests that selective laser patterning of multilayered OLED stacks is possible using UV excimer or UV and visible picosecond DPSS lasers. Transparent ITO anode films on inorganic barrier layers or metal cathode on organic OLED layers can be cleanly removed without damage to the underlying layers most likely by a thermoelastic stress-assisted low temperature ablation process.

## 7. Acknowledgements

The authors gratefully acknowledge financial support within EU program FP7 Fast2light, ICT-3, No216641, Coherent Scotland Ltd, (Glasgow, UK) and Microbridge Services Ltd (Cardiff, UK) for access to their lasers and metrology equipment and helpful discussions with Piet Bouten, Philips Research (Eindhoven, NL) and Peter Van de Weijer, Philips Research Laboratories, for providing access to Ca test equipment.

## 8. References

- [1] J.H. Burroughs, D.D.C. Bradley, A.R. Brown, R.N. Marks, K. Mackay, R.H. Friend, P.L. Burn, A.B. Holmes, *Nature* **1990**, *347*, 539-541
- [2] M.A. Baldo, D.F. O'Brien, Y. You, A. Shoustikov, S. Sibley, M.E. Thompson, S.R. Forrest, *Nature* **1998**, *395*, 151-153
- [3] D. Fyfe, *Nature Photonics* **2009**, *3*, 453-455
- [4] EU FP7 ICT-3 Collaborative Program FAST2LIGHT No 216641, [www.fast2light.org](http://www.fast2light.org)
- [5] J.D. Affinito, M.E. Gross, C.A. Coronado, G.L. Graft, I.N. Greenwell, P.M. Martin, *Thin Solid Films* **1996**, *290-291*, 63-67
- [6] S.R. Forrest, *Nature* **2004**, *428*, 911-918
- [7] H. Sirringhaus, T. Shimoda, *MRS Bulletin* **2003** 802-806
- [8] D. Lidzey, M. Voight, C. Gibeler, A. Buckley, J. Wright, K. Boehlen, J. Fieret, R. Allott, *Org. Electr* **2005**, *6*, 221-231
- [9] J.J. Brondijk, X. Li, H.B. Akkerman, P.W.M. Blom, B. de Boer, *Appl Phys A* **2009** *95*, 1-5
- [10] S.H. Ko, H. Pan, S. Ryu, N. Misra, C. P. Grigoropoulos, H.K. Park, *Appl. Phys. Lett.* 2008, *93*, 151110-1-151110-3
- [11] G. Paltauf, P.E. Dyer, *Chem.Rev.* **2003**, *103*, 487-518
- [12] E. Leveugle, D.S. Ivanov, L.V. Zhigilei, *Appl. Phys. A*, **2004**, *79*, 1643-1655
- [13] G. Nisato, P. Bouten, P. Slikkerveer, W. Bennett, G. Graf, N. Rutherford, and L. Wiese, *Proc. Asia Display* **2001**, 1435
- [14] D. Karnakis, A.J. Kearsley, M. Knowles, *J. Laser Micro/Nanoeng.*, **2009**, *4*, 218-223
- [15] P.E. Dyer, D. Karnakis, P.H. Key, D. Sands, *Appl.Surf.Sci.*, 1997, *109/110*, 168-174
- [16] P.B. Corkum, F. Brunel, N. Sherman, T. Srinivasan-Rao, *Phys.Rev.Lett.*, **1988**, *61*, 2886-2889
- [17] Z. Lin, L.V. Zhigilei, V. Celli, *Phys.Rev.B*, **2008**, *77*, 075133-1 to 075133-16
- [18] J.K. Chen, J.E. Beraun, C.L. Tham, *Int.J.Eng.Sci.* **2004**, *42*, 793-805